IEEE Access
Multidisciplinary | Rapid Review | Open Access Journal

Received August 10, 2020, accepted August 26, 2020, date of publication August 31, 2020, date of current version September 11, 2020.

Digital Object Identifier 10.1109/ACCESS.2020.3020258

Coupled Circuit and Magnetic Model for a Transverse Flux Permanent Magnet Linear Motor

DONGSHAN FU[1], (Member, IEEE), JINLIN GONG[2], (Member, IEEE), YANLIANG XU[2], FREDERIC GILLON[3], AND NICOLAS BRACIKOWSKI[4]

[1]Jiangsu Province Laboratory of Mining Electric and Automation, China University of Mining and Technology, Xuzhou 221008, China
[2]School of Electrical Engineering, Shandong University, Jinan 250061, China
[3]Ecole Centrale de Lille, Engineering School of Arts et Métiers ParisTech, University of Lille, 59000 Lille, France
[4]IREENA Laboratory, University of Nantes, 44600 Saint-Nazaire, France

Corresponding author: Yanliang Xu (xuyanliang@sdu.edu.cn)

This work was supported in part by the Fundamental Research Funds for the Central Universities under Grant 2020QN66.

ABSTRACT In this paper, a strong coupling between magnetic and electric phenomena is provided allowing to have an accurate and high-speed coupled model. A coupled circuit and magnetic model for an E-core transverse flux permanent magnet linear motor (TFPMLM) is proposed, which has an advantage linked to reducing time computing more than ten times when compared to 3-D finite-element model (FEM). Firstly, a multi-plane flexible-mesh nonlinear equivalent magnetic network (EMN) model is proposed to improve the computation efficiency as well as the high precision of the magnetic model. And a new method to define the converged iterative process is presented to further decrease the computing time. Secondly, the magnetic circuit and electric circuit are normalized into a solution matrix by introducing controlled sources and discretization methods which forms the coupled model. Then, the magnetic flux in the magnetic circuits and the current in the electric circuits are obtained simultaneously for each time step. The characteristics such as the air-gap flux density distribution, output thrust force waveforms and the phase currents are analyzed by the proposed coupled model. The modeling approach is approved by comparison with the 3-D FEM model. Finally, the proposed model is validated through the experimental setup with the machine prototype.

INDEX TERMS Coupled model, electric circuit, equivalent magnetic network (EMN), linear motor, transverse flux.

I. INTRODUCTION

Transverse-flux permanent magnet linear motor (TFPMLM) is being focused more and more in recent years, due to the advantages of high acceleration, high operating life, high force density, high fault-tolerant ability, and decoupling between electric loading and magnetic loading [1]. And the growing interest in linear motor systems requires new design approaches which take into account the drive and motor design at the same time. Coupled circuit and magnetic model efficiency and precision is very important for the design of electric machine systems [2], [3]. However, TFPMLM normally suffers from the complex structure resulting from the 3-D magnetic circuit, which is usually analyzed using 3-D FEM with time-consuming problem [4]. A coupled circuit and magnetic model of TFPMLM need to deal with two parts: magnetic part and coupled circuit part. For the magnetic part, an efficient and accurate motor analysis model is required. For the coupled circuit part, proper coupling method is another key to achieving an accurate and useful model. Linear motors have many mechanical asymmetries that induce dissymmetry magnetic and electric phenomena it is why the modelling is especially difficult.

There are some motor analysis models already used for analysis and design of TFPMLM. The analytical method [5] is adopted only in preliminary design and in understanding relationships between the parameters with brief time but low precision. Schwarz-Christoffel (SC) conformal mapping technique is another analytical method that is used to resolve the air gap field distribution and can consider the slotting

The associate editor coordinating the review of this manuscript and approving it for publication was Atif Iqbal.

effects and the end effects. This method has been applied to analyze TFPMLM [4]. However, SC method cannot take nonlinear BH curve into account, and only calculates the magnetic values in the air gap region. 3D FEM has been proved valuable in the design, performance evaluation and optimization of electrical machine with complex structure such as TFPMLM, with high precision, unfortunately also with the penalty of model establishment difficulty and long computing time. The equivalent magnetic circuit (EMC) has been used for analyzing electrical machines for many years and great progress have been made [6]–[8]. Both the nonlinearity and slot effects can be considered in those EMC models. However, the complex flux distribution in the tooth tip was carelessly handled since the tooth tip was merely simplified down to one permeance [9]. Besides, a big barrier occurs in the analysis of machines with large, variable or irregular air-gap. It is hard to determine the air-gap flux paths and the permeance calculations precisely [10]. In order to overcome the above problem, equivalent magnetic network (EMN) was developed in both 2-D magnetic circuit machines [11]–[14] and 3-D magnetic circuit machines [15]. However, a large number of mesh elements are needed to fit the topology of the electric machines with large size and irregular structure, which lead to serious computational cost especially the 3-D magnetic circuit machines. In our previous work [16], a multi-plane EMN model without flexible-mesh method and simplified winding had been proposed. This paper improved and proposed a multi-plane flexible-mesh nonlinear EMN model with a new method to define the converged iterative process to quickly analyze the TFPMLM with 3-D magnetic circuit efficiently and accurately.

Many kinds of modeling techniques for coupled circuit and magnetic exist in literature. In [2] and [3], a coupled circuit and magnetic fast model for high-speed permanent-magnet drive design is presented. And the magnetic model is a 2D analytical subdomain model which consists of solving the Maxwell equations in different regions by applying boundary conditions. Reference [17] presents a universal coupled-circuit model of a Brushless Doubly-Fed Machine (BDFM) with a high calculating speed. The above-mentioned papers just select the analytical model which not considering the nonlinear material, and only steady-state results are obtained without transient results. In [18], a multi-physic lumped model of a synchronous machine is presented. The magnetic circuit was modeled by permeance network (PN) and a ''mesh analysis'' using Kirchhoff's Voltage Law (KVL) is used. The magnetic circuit used a strong coupling with the electrical circuit. But the analytical method was used to calculate air-gap permeance because the analytical formulation is easily configurable and quick. Reference [19] proposes a coupled circuit model based on a reluctance network (RN) model. In this model, ''nodal analysis'' using Kirchhoff's Current Law (KCL) was used to solve the circuit. Therefore, the electrical circuit and magnetic circuit in the model have the same ground, which does not really exist. In order to take into account, the variation period and the phase shift between the teeth, [19] use analytical functions for the air gap reluctance calculation. Reference [20] proposes a real-time equivalent magnetic circuit (EMC) machine model to accurate electromagnetic device characteristics calculation. By considering only the main flux path of the machine, the possible mesh paths are reduced to one per phase. For sum up, the PN model, RN model and EMC model require the designers to identify structures with main flux paths and possible leakage flux paths in the air gap. Therefore, the air-gap model needs to be modified dynamically in accordance with the mover position, which is not conducive to minimize complexity and speed up the computation. The above-mentioned works just select the analytical model for the airgap field dynamic calculation. Furthermore, the above-mentioned electric machines are of 2D magnetic circuit structures, which is much easier to obtain the motor model than the TFPMLM.

Therefore, this paper proposed coupled model of TFPMLM by introducing controlled sources with discretization methods to normalize the magnetic circuit and electric circuit into a matrix. For the magnetic part, a multi-plane flexible-mesh nonlinear EMN model is proposed. The motor has been meshed, by giving the reluctance value to each mesh element to determine the material of the mesh element and then the position of the motor stator and rotor, the nodes between each mesh element and the mesh element remain unchanged. Therefore, when calculating the dynamic performance of the motor, it is not necessary to re-meshed, only the reluctance of each mesh element during the dynamic can be calculated. this method has fewer meshed elements than FEM and does not require repeated mesh, so the calculation time and meshing time are less than FEM. At the same time, the method can take into account changes in magnetic flux leakage and the internal magnetic flux path of the motor. Thus, the precision of the proposed method is higher than the EMC. Moreover, to further decrease the computing time, a new method to define the converged iterative process is presented. For the coupled circuit part, the electric circuit is directly connected with the multi-plane flexible mesh EMN to form an equivalent circuit network by introducing a controlled source. building a solution matrix of the equivalent circuit network by discretization methods to obtain the coupled model which calculate the magnetic flux and current simultaneously with an accurate and high-speed. Compared with 3D FEM, the coupled model reduces time computing more than ten times with an accepted accurate.

This paper is organized as follows: The E-core TFPMLM is briefly presented, then the EMN model with flexible mesh is described in Section II. In Section III, the electric model and coupling method are developed. In Section IV, the 3D FEM and experiments are conducted to verify the proposed model. Finally, some conclusions are drawn in Section V.

II. MAGNETIC MODEL OF THE TFPMLM

A. MACHINE TOPOLOGY AND PRINCIPLE

Fig. 1 shows the fundamental configuration of the novel three-phase E-core TFPMLM [21], which consists of two

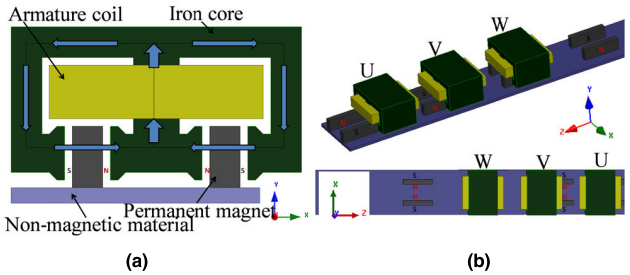

FIGURE 1. The configuration of proposed three-phase TFPMLM. (a) Cross sectional view of one phase and (b) View configuration along the moving direction (Z direction).

main parts: the armature one and the field one, as the mover and stator respectively. One armature unit is composed of an E-core and a concentrated coil wound in the middle tooth of the core. The field unit is constituted by two magnets fixed in a nonmagnetic material plate and magnetized in opposite directions as shown in Fig. 1. Armature units and magnet units are all arranged along the moving direction (z-axis), as shown in Fig. 1(b). Each field unit is separated by 180 electrical degrees and each armature unit is spatially separated by 120 electric degrees to form a three-phase system. By applying 3-phase symmetric currents into the 3-phase armature winding (one winding means one coil in Fig. 1), the proposed TFPMLM can work as a 3-phase AC synchronous machine.

B. EMN MODEL AND BASIC BLOCK ELEMENT

Due to 3-D flux distribution, modeling of the TFPMLM is quite different from the traditional linear motor. Compared to the traditional linear motor in which the magnetic flux lies largely in planes which are parallel to the direction of motion, the TFPMLM have flux paths lying transversely to this direction. The E-core TFPMLM is symmetric both in structure and magnetic flux path, and the E-core TFPMLM can be simplified to the C-shape one for quickly calculations.

The C-shape TFPMLM can be decomposed into four parts, P1, P2, N1 and N2 as shown in Fig. 2(b) and Fig. 2(c). The P1 part consists in the air gap, the permanent magnet and the iron core. P2 part consists of the winding and iron. N1 and N2 parts consist of the part yoke iron. In each part, the main magnetic flux is in planes and parallel to the direction of motion. From Fig. 2(b), It is easier to obtain the EMN model of the TFPMLM shown in Fig. 2(c).

As shown in Fig. 3, the P1, P2, N1, N2 planes are unfolded in one plane named P plane. The way to do is original and allows to take into account an important part of 3D effects of this kind of machine. The P plane is meshed into M rows and N columns to provide a unique matrix.

In a plane, a basic element of the model is reluctance block which is bi-directional i.e. flux paths in one block are assumed to only flow in 2 orthogonal directions. In this case they are radial and tangential directions. As a result, one block contains four reluctances and magnetomotive forces (MMF) in two directions. Fig.4 shows a basic block with an MMF source having thickness L_w width l_a, and height h.

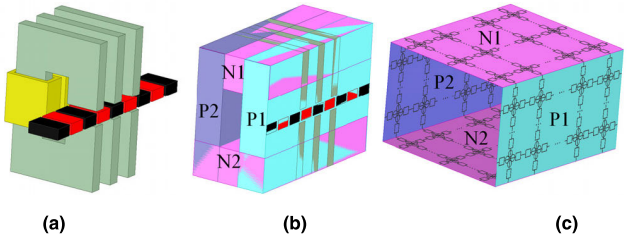

FIGURE 2. The equivalent transformation (a) The C-shape TFPMLM (b) Decomposed into four parts P1, N1, P2, N2 and (c) The EMN model of the TFPMLM decomposed in four planes modeling and linked together to provide a unique plane P.

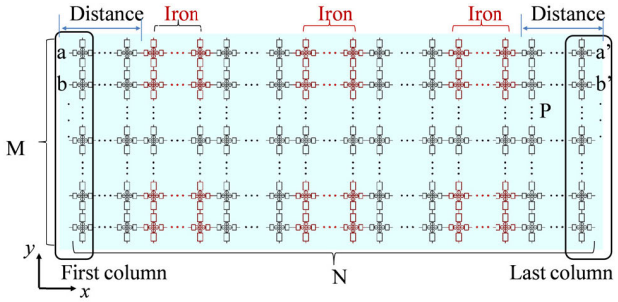

FIGURE 3. The unfold EMN model of the TFPMLM as plane P.

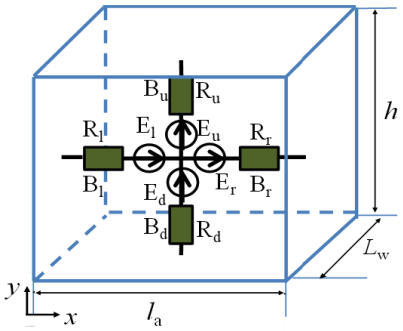

FIGURE 4. Mesh element -basic block in a plane.

The thickness of P plane elements can be written as a matrix, ie. $[\boldsymbol{L_w}] = [\, L_{P1}, L_{N1}, L_{P2}, L_{N2}]$.

Reluctance calculations for individual components in a block are given by:

$$R_u = R_d = \frac{h}{2 \cdot \mu_r \cdot \mu_0 \cdot (l_a \cdot L_w)} \tag{1}$$

$$R_l = R_r = \frac{l_a}{2 \cdot \mu_r \cdot \mu_0 \cdot (h \cdot L_w)} \tag{2}$$

where μ_r is the relative permeability of the block material, μ_0 is the permeability of the vacuum. l_a, L_w and h are the size parameters of mesh element as shown in Fig. 4.

MMF source is related to magnet and coils current. For the magnet, the equivalent MMF expressed by:

$$E_{pm} = \frac{h_m}{\mu_r \cdot \mu_{rm}} . B_r \tag{3}$$

where B_r is the residual magnetic flux density, h_m is the thickness of PM of meshed element along the magnetic flux, μ_{rm} is relative permeability of PM.

A coil of N_{e} turns carrying a current i is equivalent to an MMF source expressed by:

$$E_{\mathrm{coil}} = N_{\mathrm{e}} i \tag{4}$$

The different windings are in the different iron cores, they are separated in current loops when the machine is meshed.

C. FLEXIBLE MESH GENERATION AND BOUNDARY CONDITIONS

The element size, such as width and height, in P plane is variable which depends on the mesh density. The P plane is meshed into M rows and N columns. The elements in the same rows has the same height, while the elements in the same columns has the same width. The element height in different rows is independent, the same to the element width in different columns. The element width can be written as $[\boldsymbol{l}_{\mathbf{a}}]_{1\times \mathrm{N}}$ and height $[\boldsymbol{h}]_{\mathrm{M}\times 1}$. Changing the height of different rows or changing the width of different columns can obtain variable element size. Then, the flexible mesh generation technique is presented.

As shown in Fig. 3, the distance between the first and the last column and iron is large enough to have few influences on the air gap magnetic field. the magnetic field in first and last column is mainly produced by magnet which can be considered to have no effect on the iron.

Furthermore, in order to make convenient to calculate the magnetic field, the first column can be virtually connected to last column directly. To do that, the point a and b are considered as a' and b' respectively, as shown on Fig. 3.

Once the EMN model built, the division of each mesh element and the nodes between each mesh element is fixed, regardless of the motion of the motor. The material of the mesh element is determined by giving the permeance value and MMF source value to each mesh element to determine the position of the moving stator of the motor and the nodes between each mesh element and the mesh element do not change. Therefore, when calculating the dynamic performance of the motor, there is no need to re-mesh, only need to calculate the magnetic permeability of each mesh element during dynamic.

D. SYSTEM MATRIX AND EQUATIONS OF EMN MODEL

Kirchhoff's voltage law is applied to solve the circuit network. In the magnetic circuit loop k as shown in Fig. 5, the MMF remains to be zero:

$$\sum_{k} E_k = 0 \tag{5}$$

One could be obtained:

$$\varphi\varphi_k \sum_{\substack{i=1\\ i\neq k}}^{n} R_{ik} - \sum_{\substack{i=1\\ i\neq k}}^{n} {}_i R_{ik} = \sum_{\substack{i=1\\ i\neq k}}^{n} \{E_{ik}\} \tag{6}$$

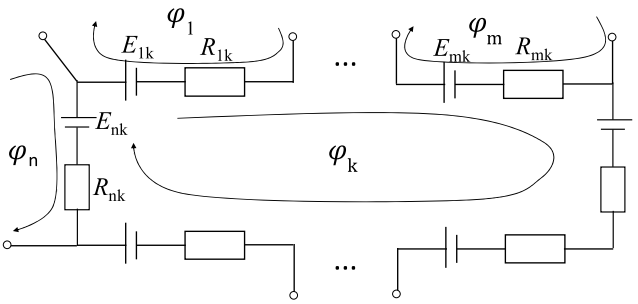

FIGURE 5. Magnetic circuit network for the loop k.

where φ_k and φ_i is the flux in the magnetic circuit loop k and i as shown in Fig. 5. And:

$$\{E_{ik}\} = \begin{cases} E_{ik} & \text{The same direction with } \varphi_k \\ -E_{ik} & \text{The different direction with } \varphi_k \end{cases} \tag{7}$$

Similarly, for all magnetic circuits' loops, (7) is generalized as (8):

$$\begin{bmatrix} \boldsymbol{R}_{11} & \cdots & \boldsymbol{R}_{1n} \\ \vdots & \ddots & \vdots \\ \boldsymbol{R}_{n1} & \cdots & \boldsymbol{R}_{nn} \end{bmatrix} \begin{bmatrix} \varphi_1 \\ \vdots \\ \varphi_n \end{bmatrix} = \begin{bmatrix} E_{s1} \\ \vdots \\ E_{sn} \end{bmatrix} \tag{8}$$

with E_{sk} is the sum of flux sources connected in circuit loop k expressed as the right-hand side of (6) and [**R**] is the reluctance matrix defined by (9)

$$\boldsymbol{R}_{ij} = \begin{cases} \pm R_{ij} & i \neq j \\ \sum\limits_{\substack{k=1\\ k\neq i}}^{n} R_{ki} & i = j \end{cases} \tag{9}$$

Noted that the R_{ij} is the sum of reluctance shared by magnetic circuit loop i and j. $\boldsymbol{R}_{ij} = R_{ij}$ with φ_i and φ_j are in the same direction, otherwise $\boldsymbol{R}_{ij} = -R_{ij}$. The size of mesh element has influences on the result accuracy and calculating speed. It is convenient to build the system matrix and the equations for the regular mesh.

From the equations above, the flux in each branch are obtained. Then, the flux density in a block are given by:

$$B_u = \frac{\varphi_u}{l_{\mathrm{a}} L_{\mathrm{w}}},\ B_r = \frac{\varphi_r}{h L_{\mathrm{w}}},\ B_l = \frac{\varphi_l}{h L_{\mathrm{w}}},\ B_d = \frac{\varphi_d}{l_a L_{\mathrm{w}}} \tag{10}$$

where φ_u, φ_r, φ_l, φ_d are the magnetic flux flowing in each element branches.

Each element has a module of flux density B_{mod}. It is a global view of the flux density deduced from a good balancing of the energy.

$$B_{mod} = \sqrt{\frac{\mathrm{B}_u^2 + \mathrm{B}_d^2}{2} + \frac{\mathrm{B}_l^2 + \mathrm{B}_r^2}{2}} \tag{11}$$

In the plane P1, where the thrust force is, it is possible to compute the radial and tangential component of the flux density B_{x}, B_{y} that is a local view:

$$B_x = \frac{1}{2}(B_l + B_r), \quad B_y = \frac{1}{2}(B_u + B_d) \tag{12}$$

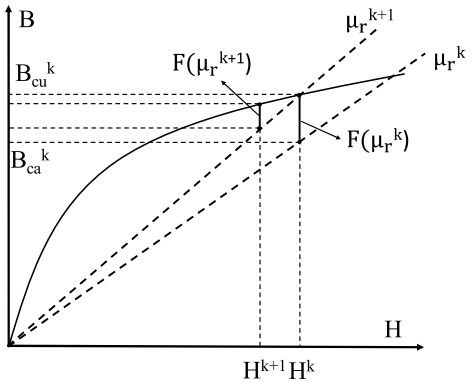

FIGURE 6. Explains of the iterative process of the magnetic model with nonlinear magnetizing curve to take into account saturation effect.

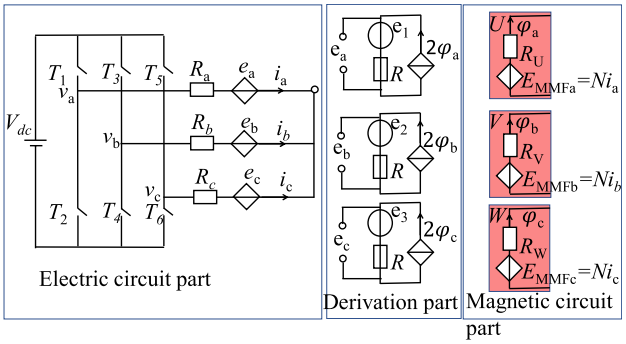

FIGURE 7. Coupled electric and magnetic model of the TFPMLM.

E. NONLINEAR ANALYSIS

Given resistance and flux source matrices, scalar magnetic fluxes are obtained by solving (8). The nonlinear characteristic of the core material presented by a magnetization curve is taken into account through a lookup table using interpolation from the magnetization curve.

Basically, Newton Raphson method is an efficient method dealing with nonlinear equation. Applying NR method to the EMN, Equation (8) is rephrased as:

$$f(\boldsymbol{\varphi}) = \boldsymbol{R\varphi} - \boldsymbol{E} = 0 \tag{13}$$

However, the NR method requires more computational efforts for the differentiation process specially to obtain the Jacobian matrix. And taking derivative of $f(\boldsymbol{\varphi})$ with respect to φ raises another difficulty since the resistance matrix $\boldsymbol{R}$ is unknown and is in fact an implicit function of $\boldsymbol{\varphi}$. Thus, several articles are using fixed point method [14].

In this paper, the iterative process is shown in Fig. 6. Based on existing absolute related permeability μ_r, the induction magnetic flux density B_{ca} can be calculated by equation (1) - (13). An equation can be written to express the relation between B_{ca} and μ_r:

$$B_{ca} = g(\mu_r) \tag{14}$$

From the kth iteration, the induction magnetic flux density B_{ca}^k, the magnetic field strength H^k can be obtained under the related permeability μ_r^k:

$$H^k = \frac{B_{ca}^k}{\mu_r^k \mu_0} \tag{15}$$

Nonlinear magnetizing curve of the core material is expressed in Fig. 6, from the magnetization curve, we can obtain the nonlinear magnetizing curve flux density B_{cu}^k with the magnetic field strength H^k which can be express as:

$$B_{cu}^k = B(H^k) \tag{16}$$

then μ_r^k is renewed as μ_r^{k+1}:

$$\mu_r^{k+1} = \frac{B_{cu}^k}{\mu_0 H^k} \tag{17}$$

Usually, the iterative process could be defined as converged at k th iteration if (18) is satisfied.

$$x = \left\| \frac{\mu_r^{k+1} - \mu_r^k}{\mu_r^k} \right\|_2 < \varepsilon \tag{18}$$

(18) means that the maximum local error between two consecutive iterations is not bigger than a predefined tolerance ε.

However, the ideal result of the nonlinear problem is to find a related permeability μ_r ensuring that the induction magnetic flux density B_{ca} equals to the nonlinear magnetizing curve flux density B_{cu}. That is to say, the basic form of nonlinear equation can be written as:

$$F(\mu_r) = B_{cu} - B_{ca} = 0 \tag{19}$$

Then, this paper proposes another way to define the converged of the iteration process. It expresses as:

$$X = \left\| F\left(\mu_r^k\right) \right\|_2 < \varepsilon \tag{20}$$

(20) means that the differences between the magnetic flux density B_{ca} and the nonlinear magnetizing curve flux density B_{cu} is not bigger than a predefined tolerance ε.

The division calculation in equation (18) above cost more time and computer sources than the subtraction calculation in equation (20).

III. ELECTRIC COUPLING

As shown in Fig. 7, the electronic and magnetic models are combined. Dissymmetric in the magnetic part induces asymmetries in electric part. It is classical for linear motor and must be taken into account to have an accurate model. The electric part shows a classic three-phase two-level inverter, where V_{dc} is the DC-bus voltage, [T1,T3,T5] (respectively T2,T4,T6) is the upper (respectively lower) MOSFETs of phases $[U, V, W]$, $[R_a, R_b, R_c]$ is the motor phase resistance, $[e_a, e_b, e_c]$ are the electromotive forces (*emf*) of phases $[U, V, W]$, $[v_a, v_b, v_c]$ are the electrical potentials of the phases $[U, V, W]$ connected to the inverter. The magnetic circuit part is composed of the EMN model. The connection between the magnetic circuit and the electric circuit is through the winding coils.

The coils around the iron core (U, V, W shown in Fig.1) are considered to establish the link between the electric currents

and the magnetomotive forces. The magnetic field in the coils allows to associate a magnetomotive force with each iron core. The current in winding coils can produce the MMF in the magnetic circuit which is expressed in (4). Similarly, the coils around the iron core are considered to establish the link between the magnetic flux and *emf*. And the changing flux in the magnetic circuit flows through the iron core can produce the *emf* in the coils.

The *emf* (e_a, e_b, e_c) for each phase of the electric circuit part are calculated by using Faraday's law of induction. The magnetic circuit part is the EMN model of C-shape. For the E-core TFPMLM, the *emf* for each phase of the electrical model are considered as the double flux (φ) flowing through the coil of the EMN model. Then the *emf* in E-core TFPMLM is given by:

$$emf = 2N\frac{d\varphi}{dt} \tag{21}$$

Discretized the equation (21) using backward Euler's rule:

$$emf = \frac{2N}{\Delta t}\varphi(\mathrm{t}) - \frac{2N}{\Delta t}\varphi(\mathrm{t}-\Delta t) \tag{22}$$

Assume $\frac{2N}{\Delta t}$ as the coupling resistance R, φ(t) as the current and $-\frac{2N}{\Delta t}\varphi(\mathrm{t}-\Delta t)$ as the voltage source Et. The equation (22) can be written as:

$$emf = R\varphi\,(\mathrm{t}) + Et \tag{23}$$

As shown in Fig. 7, the coupled circuit model is decomposed into three parts, it is electric circuit part, derivation part and magnetic circuit part. Each part connected through the controlled power source. the magnetomotive forces (E_{MMFa}, E_{MMFb}, E_{MMFc}) in magnetic part produced by the phase current (i_a, i_b, i_c) is considered as a current controlled voltage source (CCVS). N is the turn number of each phase winding. The magnetic circuit part (φ_a, φ_b, φ_c) connected with the derivation part ($2\varphi_a$, $2\varphi_b$, $2\varphi_c$) uses current controlled current source (CCCS). The derivation part (e_a, e_b, e_c) connected with the electric circuit part (*emf*) uses voltage controlled voltage source (VCVS). By using the control source, the different parts of the coupling model remain independent. However, if the node voltage method is used to solve the coupling model, a virtual resistor is needed to connect the circuit and the magnetic circuit. Then, this paper uses the loop current method to solve the coupled model.

Simplified the inverter to a three-phase voltage source as shown in Fig. 8. And the loop current method is applied to solve the electric circuit network. The equation of electric model part is:

$$\begin{aligned}&(R_a + R_b)\,I_1 + R_b I_2 + \frac{2N}{\Delta t}\varphi_a\,(t) - \frac{2N}{\Delta t}\varphi_b\,(t)\\ &= v_a - v_b + \frac{2N}{\Delta t}\varphi_a\,(t-\Delta t) - \frac{2N}{\Delta t}\varphi_b\,(t-\Delta t) = U_1\end{aligned} \tag{24}$$

$$\begin{aligned}&R_b \mathrm{I}_1 + (R_b + R_c)\,\mathrm{I}_2 - \frac{2N}{\Delta t}\varphi_b\,(\mathrm{t}) + \frac{2N}{\Delta t}\varphi_c\,(\mathrm{t})\\ &= v_c - v_b + \frac{2N}{\Delta t}\varphi_c\,(\mathrm{t}-\Delta t) - \frac{2N}{\Delta t}\varphi_b\,(\mathrm{t}-\Delta t) = U_2\end{aligned} \tag{25}$$

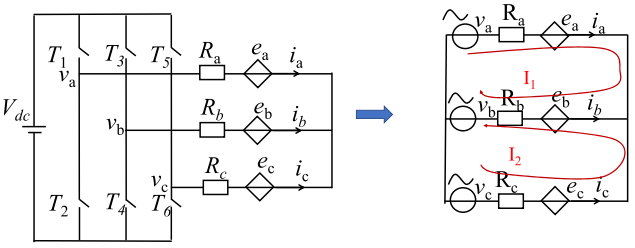

FIGURE 8. The Simplified inverter to a three-phase voltage source.

Note that:

$$I_1 = i_a;\ I_2 = i_c;\quad \text{and}\ \ i_b = -i_a - i_c \tag{26}$$

where φ_a, φ_b, φ_c are the fluxes in the different phase windings. The left part of (24) and (25) are the fluxes and phase current, the right part of (24) and (25) are the voltage sources which can be represented by U_1 and U_2 for simplify.

Combining the equation (4), (5), (8), (26), the EMN model system matrix can be expressed as:

$$\begin{bmatrix} \boldsymbol{R}_{11} & \cdots & \cdots & \boldsymbol{R}_{1n} & \vdots & \vdots \\ \vdots & \ddots & \cdots & \vdots & N_a & 0 \\ \vdots & \ddots & \ddots & \vdots & \vdots & \vdots \\ \vdots & \ddots & \ddots & \vdots & -N_b & -N_b \\ \vdots & \ddots & \ddots & \vdots & \vdots & \vdots \\ \vdots & \ddots & \ddots & \vdots & 0 & N_c \\ \vdots & \ddots & \ddots & \vdots & \vdots & \vdots \\ \vdots & \ddots & \ddots & \vdots & 0 & 0 \\ \boldsymbol{R}_{n1} & \cdots & \ddots & \boldsymbol{R}_{nn} & \vdots & \vdots \end{bmatrix} \begin{bmatrix} \varphi_1 \\ \vdots \\ \varphi_n \\ I_1 \\ I_2 \end{bmatrix} = \begin{bmatrix} E_1 \\ \vdots \\ E_n \end{bmatrix} \tag{27}$$

The system matrix consists of the reluctance matrix $\boldsymbol{R}$ combined with the number of turns matrix $\boldsymbol{N}$, the loop current column vector φ combined the loop flux and the phase current, and the driving column vector $\boldsymbol{E}$. the magnetomotive forces $E_1, \ldots, E_n$ are produced by the permanent magnet. N_a, N_b, N_c are the turn number of each phase, and in this paper, $N = N_a = N_b = N_c$. The magnetomotive forces produced by the current in winding coils are in left part of the (27).

Combining the equation (24), (25), (27), the coupled model system matrix equation can be expressed as:

$$[\boldsymbol{R}_c] \begin{bmatrix} \varphi_1 \\ \vdots \\ \varphi_n \\ I_1 \\ I_2 \end{bmatrix} = \begin{bmatrix} E_1 \\ \vdots \\ E_n \\ U_1 \\ U_2 \end{bmatrix} \tag{28}$$

where the details of coupled model resistance matrix $[\boldsymbol{R}_c]$ are shown in Fig. 9. $[\boldsymbol{R}_c]$ composed of four parts: the reluctance

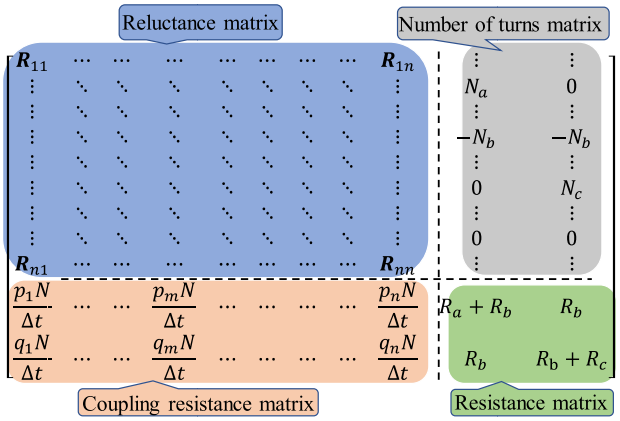

FIGURE 9. The coupled model resistance matrix-[R_c].

matrix, the number of turns matrix, the resistance matrix, the coupling resistance matrix. the reluctance matrix and number of turns matrix are from EMN model system matrix equation (27), the resistance matrix is the resistance of the electric part, the coupling resistance matrix is from (24) and (25), however, $\varphi_1 \ldots \varphi_n$ in the loop current column vector $\boldsymbol{\varphi}$ is the loop flux as shown in Fig. 5. And the flux in each phase can calculate from the loop flux. In the coupled model, the equation (24) and (25) satisfied by add the coefficient $p_1 \ldots p_n$ and $q_1 \ldots q_n$ which satisfy:

$$\begin{bmatrix} p_1 & \cdots & p_n \\ q_1 & \cdots & q_n \end{bmatrix} \begin{bmatrix} \varphi_1 \\ \vdots \\ \varphi_n \end{bmatrix} = \begin{bmatrix} 2\varphi_a - 2\varphi_b \\ -2\varphi_b + 2\varphi_c \end{bmatrix} \tag{29}$$

The system matrix equation consists of the coupled model reluctance matrix [$\boldsymbol{R}_c$], the flux current and electric current column vector, and the driving column vector. the coupled model reluctance matrix [$\boldsymbol{R}_c$] is just two dimensions bigger than the EMN model reluctance matrix $\boldsymbol{R}$.

IV. 3-D FEM AND EXPERIMENT VERIFICATION

A. PROTOTYPE AND EXPERIMENTAL PLATFORM

Fig. 10 shows all the design variables to define a specific topology of the TFPMLM. Table 1 presents a summarization of the design specification of the TFPMLM in which a three-phase prototyped one is fabricated.

The prototyped TFPMLM and test platform is shown in Fig. 11(a), which features a short armature mover of only three units, and a longer field stator. The prototyped TFPMLM is tested, 3D FEM-based and EMN calculated for its air gap flux density distributions, EMF waveforms, force waveforms when it is at no-load and load. The no-load test platform, shown in Fig. 11(b), consists mainly of the prototyped TFPMLM, force meter and prime mover. The prime mover is used to push the prototyped motor. The force meter is sandwiched between the prime mover and the prototype. The load test platform is shown in Fig. 11(c).

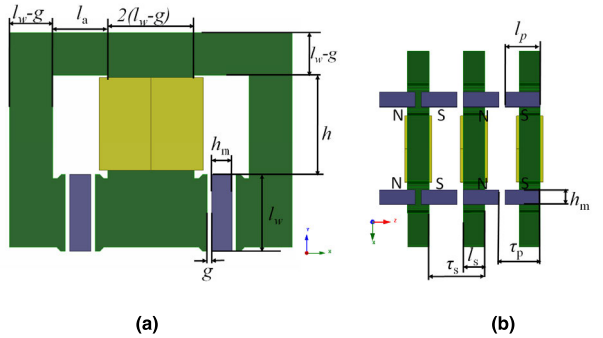

FIGURE 10. Structural parameter labels of the TFPMLM(a) x-y coordinate and (b) x-z coordinate.

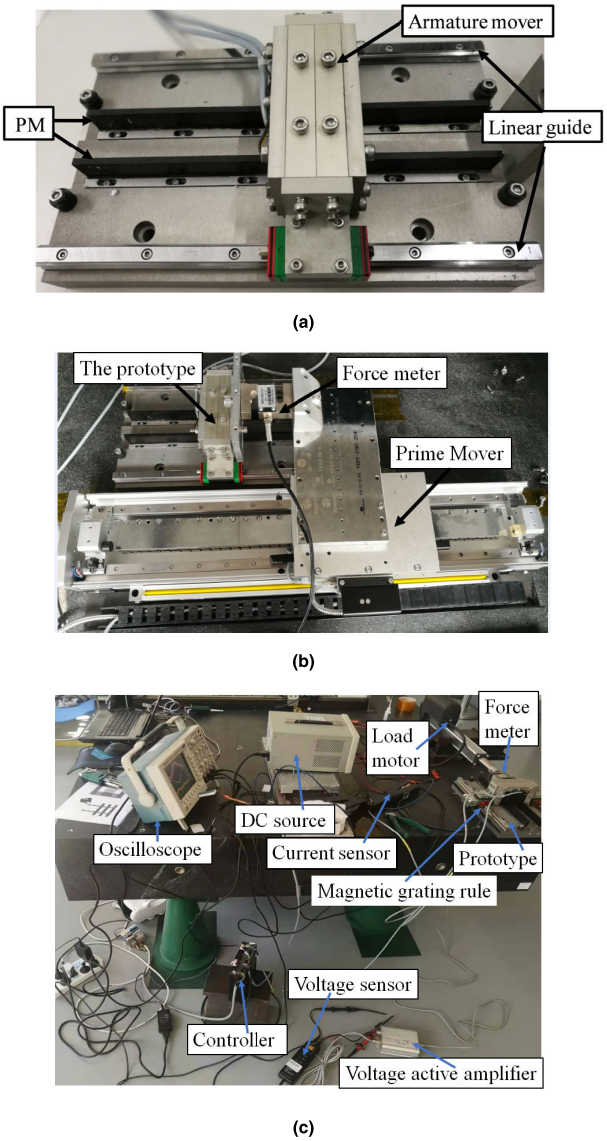

FIGURE 11. The prototyped and test platform. (a)The prototyped of TFPMLM. (b) The no-load test platform. (c) The load test platform.

B. EMN MODEL

The Fig. 12. shows the meshed model of the TFPMLM based on EMN method Fig. 13 shows the flux density distributions under the excitation of PM. The EMN model take the B-H

TABLE 1. Data of the protype.

Symbol	Quantity	Symbol	Quantity
Pole pitch τ_p (mm)	13.5	Air gap length g (mm)	1
Magnet height l_p (mm)	11.5	Magnet Magnetization h_m (mm)	5
Magnet width l_w (mm)	18	Armature slot pith τ_s (mm)	18
Armature slot height h mm	14	Armature slot width l_a (mm)	13
E-core width l_s (mm)	7		
Number of turns N of phase winding	300	Magnets: NdFeB Br=1.3T, Hc=890kA/m	

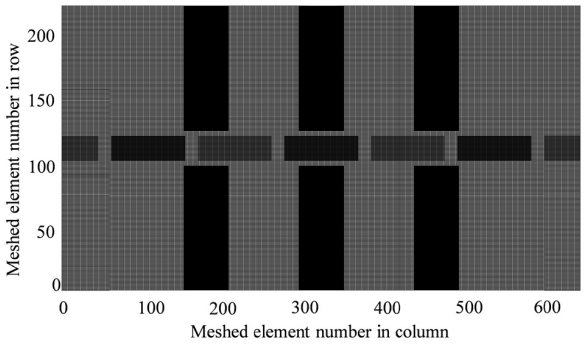

FIGURE 12. The EMN model of the TFPMLM.

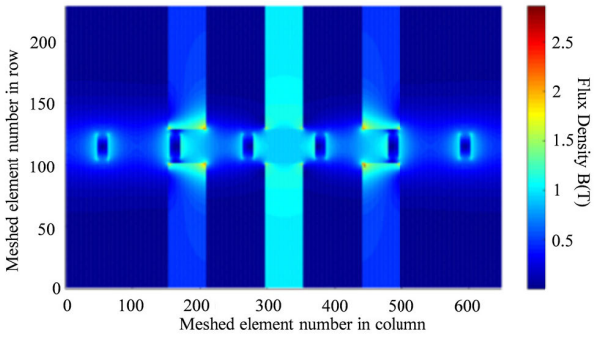

FIGURE 13. The flux density distributions under the excitation of PM.

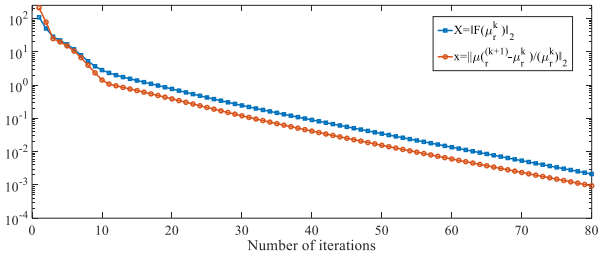

FIGURE 14. The norm of local error between two consecutive iterations.

curves into considerations, Fig. 14 shows the value of the two error between two consecutive iterations x and the differences between the magnetic flux density X. From the Fig. 14, it proves that the two methods to define whether the iterative process has converged is feasible.

Fig. 15, shows the air gap field flux distributions of the TLPMLM obtained by EMN and 3D FEM respectively. The field is obtained at no load. The related position of winding cores and permanent magnet can be seen in Fig. 15. It can be

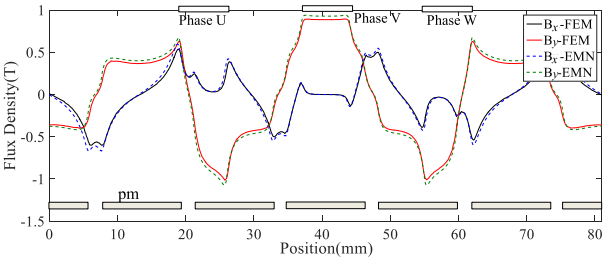

FIGURE 15. The air gap field flux distributions of the TLPMLM.

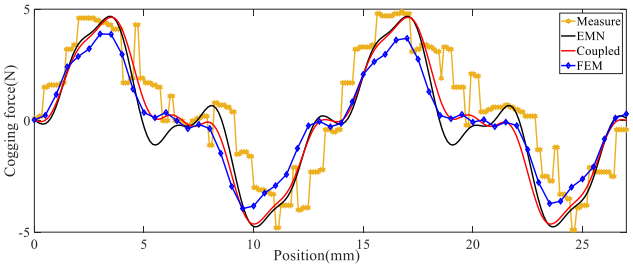

FIGURE 16. The cogging force comparison obtained from experiment, EMN model, coupled model and 3D FEM.

seen that the magnetic flux density from EMN closely follows the result of 3D FEM. The maximum error between the curve's comparisons is 6 percent. The magnetic flux density from EMN are the average value of the mesh elements which does not reflect the sharp change in magnetic density.

C. EXPERIMENTAL VERIFICATION

To validate the proposed EMN model and coupled model of the TFPMLM, 3-D FEM model and experiment platform has been built.

The cogging force is obtained from experiment, EMN model, coupled model and 3D FEM is given in Fig. 16. In Fig 16, the difference between 3D FEM and the proposed model is the result of the 2D meshed in p plane of EMN method that does not consider the 3D flux path. In addition, the 3D FEM result is not good enough due to the number of mesh elements being limited by computer performance. The thrust force is obtained when it runs at id = 0, iq = 3A. In Fig 17, the thrust force obtained from proposed EMN model, 3D FEM and experimental. At the position about 3-8 and 15-20 has same error which is caused by the added 3D flux path that EMN method does not consider. The average thrust force from FEM, EMN and experiment are 76.7N, 75.3N and 79.8N. It can be seen that the thrust values calculated by each model are very close. It is indicated that the analysis models proposed in this paper have high precision.

The three-phase on-load EMF waveform results based on 3D FEM, experiment and proposed model are shown in Fig. 18 respectively, when the motor moves in a constant speed of 1m/s. under the following conditions: at no load, means that the three phase windings are open-circuited and in the coupled model, the voltage v_a, v_b, v_c are zero and meanwhile the resistances R_a, R_b, R_c are infinity, in this paper, $R_a = R_b = R_c = 30k\Omega$. It can be seen from Fig. 18 that the

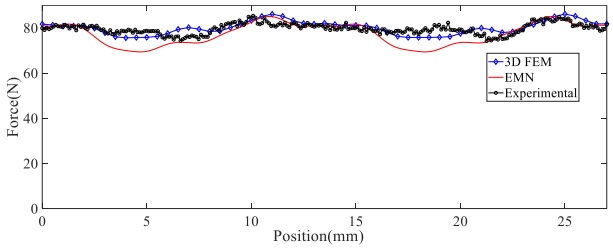

FIGURE 17. The thrust force comparison obtained from EMN model, 3D FEM and experiment.

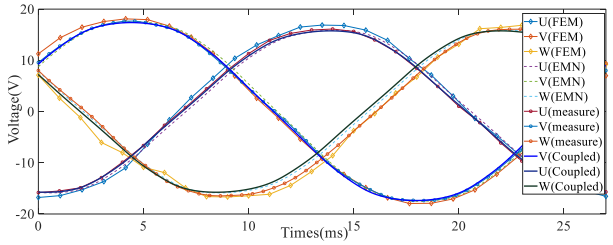

FIGURE 18. EMF results when the mover moves in a constant speed of 1 m/s.

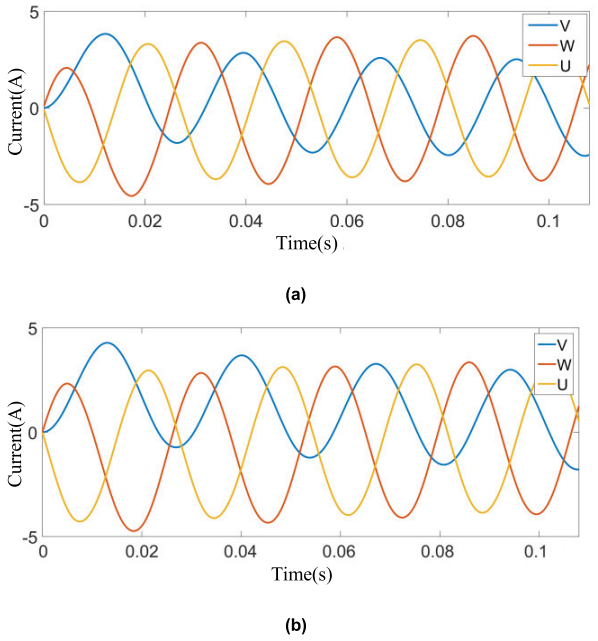

FIGURE 19. The instantaneous current under the voltage source. (a) Coupled model, (b) 3-D FEM.

results from coupled model, EMN, 3D FEM and experiment are much coincided with each other. It can be seen that the EMF value of phase V is slightly bigger than the phase U and phase W due to the end effect.

The instantaneous three phase current obtained from the coupled model and 3-D FEM under the three-phase sine voltage source as shown in Fig. 19(a) and Fig. 19(b). The amplitude of the voltage is about 30V and the phase is same to the no-load EMF, and the mover moves in a constant speed of 1 m/s. The instantaneous three phase current is asymmetrical alternating electric current because from the EMF value of phase V is slightly bigger than the phase U and phase W due to the end effect which is mentioned above. And Table 2 presents the detail specifications of coupled model and 3D FEM such as the mesh size, step and stop time and computation times of the TFPMLM. The consuming time of coupled model is about 73.6 minutes which is at least ten times less than 3D FEM cost about 941 minutes even if the coupled model has a smaller step time, a larger number of mesh elements. In addition, the coupled model only costs no more than 1 Gigabytes of memory instead of 16 Gigabytes of 3D FEM.

TABLE 2. Specifications and simulation time.

MOdel	Step time(ms)	Stop time(ms)	Number of mesh elements	Consuming time(min)
Coupled model	0.0625	108	147744	73.6
3D FEM	0.08	108	97333	941

V. CONCLUSION

In this paper, a coupled electric and magnetic model for a novel E-core transverse flux permanent magnet linear motor is proposed. The multi-plane flexible-mesh EMN model is proposed to analysis the magnetic part of the motor. The nonlinear iterative process, multi-plane flexible-mesh method were also presented. The normalization of electric model and magnetic model is described. To verify the accuracy of the proposed models, several simulations are applied to our TFPMLM and compared with experimental results and 3-D FEM. The results from proposed models, 3-D FEM and experimental are in good agreement. The primary contribution of this work is the coupled model methodology; more specifically, the proposed coupled model contributes higher efficiency and lighter computational loads with a high accurate when compared to commercially available modeling techniques adhering to similar time constraints.

REFERENCES

[1] M. Zhao, Y. Wei, H. Yang, M. Xu, F. Han, G. Deng, D. Hou, and P. Zhang, "Development and analysis of novel flux-switching transverse-flux permanent magnet linear machine," *IEEE Trans. Ind. Electron.*, vol. 66, no. 6, pp. 4923–4933, Jun. 2019.

[2] M. Gerber, A. Gilson, D. Depernet, F. Dubas, C. Espanet, and G. Andrieux, "Coupled electronic and magnetic fast simulation for high-speed permanent-magnet drive design," in *Proc. IEEE Vehicle Power Propuls. Conf. (VPPC)*, Hangzhou, China, Oct. 2016, pp. 1–6.

[3] M. Gerber, A. Gilson, F. Dubas, and C. Espanet, "Coupled circuit and magnetic fast model for high-speed permanent-magnet drive design," *IET Electr. Syst. Transp.*, vol. 8, no. 1, pp. 27–34, Mar. 2018.

[4] D. Fu, Y. Xu, F. Gillon, J. Gong, and N. Bracikowski, "Presentation of a novel transverse-flux permanent magnet linear motor and its magnetic field analysis based on Schwarz–Christoffel mapping method," *IEEE Trans. Magn.*, vol. 54, no. 3, Mar. 2018, Art. no. 6000204.

[5] J.-S. Shin, R. Watanabe, T. Koseki, and H.-J. Kim, "Practical design approach of a transverse flux linear synchronous motor for compact size, small mover weight, high efficiency, and low material cost," *IEEE Trans. Magn.*, vol. 51, no. 3, pp. 1–4, Mar. 2015.

[6] S. Zhou, H. Yu, M. Hu, C. Jiang, and L. Huang, "Nonlinear equivalent magnetic circuit analysis for linear flux-switching permanent magnet machines," *IEEE Trans. Magn.*, vol. 48, no. 2, pp. 883–886, Feb. 2012.

[7] B. Sheikh-Ghalavand, S. Vaez-Zadeh, and A. Hassanpour Isfahani, "An improved magnetic equivalent circuit model for iron-core linear permanent-magnet synchronous motors," *IEEE Trans. Magn.*, vol. 46, no. 1, pp. 112–120, Jan. 2010.

[8] E. Kazan and A. Onat, "Modeling of air core permanent-magnet linear motors with a simplified nonlinear magnetic analysis," *IEEE Trans. Magn.*, vol. 47, no. 6, pp. 1753–1763, Feb. 2011.
[9] G. Liu, L. Ding, W. Zhao, Q. Chen, and S. Jiang, "Nonlinear equivalent magnetic network of a linear permanent magnet Vernier machine with end effect consideration," *IEEE Trans. Magn.*, vol. 54, no. 1, pp. 1–9, Jan. 2018.
[10] G. Liu, S. Jiang, W. Zhao, and Q. Chen, "Modular reluctance network simulation of a linear permanent-magnet Vernier machine using new mesh generation methods," *IEEE Trans. Ind. Electron.*, vol. 64, no. 7, pp. 5323–5332, Jul. 2017.
[11] C. Bruzzese, D. Zito, E. Santini, and A. Tessarolo, "A finite reluctance approach to electrical machine modeling and simulation: Magnetic network-based field solutions in MATLAB environment," in *Proc. 40th Annu. Conf. IEEE Ind. Electron. Soc.*, Dallas, TX, USA, Oct. 2014, pp. 323–329.
[12] T. Hosoi, K. Shima, and T. Fukami, "Magnetic circuit analysis of permanent-magnet-assisted salient-pole synchronous machines under steady states," *IEEE Trans. Ind. Appl.*, vol. 48, no. 3, pp. 895–902, May 2012.
[13] M. Rottach, C. Gerada, T. Hamiti, and P. W. Wheeler, "A computationally efficient design procedure for actuator motors using magnetic reluctance- and thermal resistance network models," in *Proc. 20th Int. Conf. Electr. Mach.*, Marseille, France, Sep. 2012, pp. 2526–2532.
[14] M. Fukuoka, K. Nakamura, and O. Ichinokura, "A method for optimizing the design of SPM type magnetic gear based on reluctance network analysis," in *Proc. 20th Int. Conf. Electr. Mach.*, Sep. 2012, pp. 30–35.
[15] J.-H. Sim, D.-G. Ahn, D.-Y. Kim, and J.-P. Hong, "Three-dimensional equivalent magnetic circuit network method for precise and fast analysis of PM-assisted claw-pole synchronous motor," *IEEE Trans. Ind. Appl.*, vol. 54, no. 1, pp. 160–171, Jan. 2018.
[16] D. Fu, F. Gillon, Y. Xu, N. Bracikowski, and J. Gong, "Equivalent magnetic network of a transverse-flux permanent magnet linear motor," in *Proc. 13th Int. Conf. Electr. Mach. (ICEM)*, Alexandroupoli, Greece, Sep. 2018, pp. 2157–2163.
[17] P. Loehdefink, A. Dietz, and A. Moeckel, "Universal coupled-circuit modelling approach applied to the brushless doubly-fed induction machine," in *Proc. 11th GMM/ETG-Symp. Innov. Small Drives Micro-Motor Syst.*, Saarbrücken, Germany, 2017, pp. 1–6.
[18] N. Bracikowski, M. Hecquet, P. Brochet, and S. V. Shirinskii, "Multiphysics modeling of a permanent magnet synchronous machine by using lumped models," *IEEE Trans. Ind. Electron.*, vol. 59, no. 6, pp. 2426–2437, Jun. 2012.
[19] H. Kien Bui, N. Bracikowski, M. Hecquet, K.-L. Zappellini, and J.-P. Ducreux, "Simulation of a large power brushless synchronous generator (BLSG) with a rotating rectifier by a reluctance network for fault analysis and diagnosis," *IEEE Trans. Ind. Appl.*, vol. 53, no. 5, pp. 4327–4337, Oct. 2017.
[20] F. E. Fleming and C. S. Edrington, "Real-time emulation of switched reluctance machines via magnetic equivalent circuits," *IEEE Trans. Ind. Electron.*, vol. 63, no. 6, pp. 3366–3376, Jun. 2016.
[21] D. Fu, Y. Xu, and J. Gong, "Presentation of E-core transverse-flux permanent magnet linear motor and its no-load magnetic field analysis based on schwarz-christoffel transformation," in *Proc. IEEE Conf. Electromagn. Field Comput. (CEFC)*, Miami, FL, USA, Nov. 2016, p. 1.

DONGSHAN FU (Member, IEEE) received the B.S. degree in electrical engineering and automation from the School of Information and Electrical Engineering, China University of Mining and Technology, Xuzhou, China, in 2013, and the Ph.D. degree from the School of Electrical Engineering, Shandong University, China, in 2019. He is currently a Lecturer with the School of Electrical and Power Engineering, China University of Mining and Technology. His research interests include design and analysis for permanent-magnet machine and special structural machine.

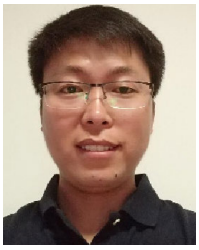

JINLIN GONG (Member, IEEE) received the B.Sc. and M.S. degrees from Southwest Jiaotong University, Chengdu, China, in 2006, the Engineering Degree from the Ecole Centrale de Lyon in 2008, and the Ph.D. degree in electrical engineering from the Ecole Centrale de Lille, France, in 2011. From October 2011 to August 2012, he was an Assistant Professor with the Engineering School of Arts et Métiers ParisTech, Lille, France. He is currently an Associate Professor with the School of Electrical Engineering, Shandong University, Jinan, China. His research interests include optimal design and control of linear machines and multiphase machines.

YANLIANG XU received the B.S. and M.Sc. degrees in electrical machines from the Shandong University of Technology, Jinan, China, in 1989 and 1994, respectively, and the Ph.D. degree in electrical machines from the Shenyang University of Technology, Shenyang, China, in 2001. He is currently a Professor with the School of Electrical Engineering, Shandong University. He is the Head of the Institute of Electrical Machine. His research interests include electrical machines, especially permanent magnet electrical machines and special electrical machines.

FREDERIC GILLON received the Engineer Diploma and Ph.D. degrees in electrical engineering from the Université des Sciences et Technologies de Lille, Lille, France, in 1992 and 1997, respectively. Since 1999, he has been an Associate Professor with the Ecole Centrale de Lille, University of Lille, Lille, France. His main research subjects are design by the optimization of electromechanical systems and special electric machines such as linear, and axial- and radial-flux synchronous motors. His second interest field is traction machine applied to railway systems or electric/hybrid vehicles.

NICOLAS BRACIKOWSKI received the B.Sc. and M.Sc. degrees in electrical engineering from the University of Artois, France, and the Ph.D. degree from the Ecole Centrale de Lille, France, in 2012. Since 2013, he has been an Associate Professor with the University of Nantes, France, where he carries out research with the IREENA Laboratory, Institut de Recherche en Energie Electrique de Nantes Atlantique. His areas of research include optimal design of electrotechnical device, multiphysics lumped models, and acoustic noise in electrical machines.